Department of Physics and Astronomy
University of Heidelberg

Bachelor Thesis in Physics
submitted by Fabian Klein

Fabian Klein

born in Trier (Germany)

1988

“Comparison of classical and quantum mechanical dynamics in ionisation processes in strong laser fields”

This Bachelor Thesis has been carried out by Fabian Klein at the
Max-Planck-Institut für Kernphysik in Heidelberg
under the supervision of
Hon.-Prof. Dr. C. H. Keitel

Abstract

In this thesis the Strang-splitting technique is used was a classical Monte Carlo simulation imitating quantum effects for the propagation of a hydrogen atom in a monochromatic laser field using dipole approximation. The pulse was imposed onto the atom for one full laser period. The treatment was done in 3 dimensions and without any changes to the potentials used (e.g. no soft-core potential). The main goal is to determine the ionisation probability in order to bring high intensity laser to proper use in science and technology as measurements of the intensity of high intensity laser are experimentally challenging. A comparison with a symplectic implicit and an explicit 3rd order Runge-Kutta scheme was able to show the advantages the Strang-splitting has over both Runge-Kutta schemes used. The comparison to a quantum mechanical numerical solution yielding upper bounds for the ionisation probability using the program Qprop could only partially verify the classical results obtained. However the problems that occurred are known and are not to be attributed to the Strang-splitting. In summary the magnificent performance of the Strang-splitting caused by its proterties (symplecticity symmetry-preserving, time-reversibility preservation and first order invariant preservation) could be verified and more research possibilities were proposed.

Zusammenfassung

In dieser Arbeit wurde die Strang-splitting Methode in einer klassischen Monte Carlo Simulation, welche Quantenverhalten für die Propagation eines Wasserstoffatoms in einem monochromatischen Laserfeld in Dipolnäherung imitiert, implementiert und getestet. Die Dauer des Laserpulses wurde zu einer vollen Laserperiode gewählt. Die Behandlung des Problems wurde in 3 Dimension durchgeführt und keine Vereinfachungen am Potential (wie z.B. ein soft-core Potential) wurden durchgeführt. Die Hauptintention war dabei die Bestimmung der Ionisationswahrscheinlichkeit, um zu erreichen, dass sehr intensitätsstarke Laser vernünftig in Wissenschaft and Technik verwandt wedren können, da die Bestimmung der Intensität für Laser hoher Intensität experimentell sehr schwierig ist. Ein Verglich mit einem symplektischen impliziten und einen expliziten Runge-Kutta Verfahren dritter Ordnung zeigt die gewaltigen Vorteile des Strang-splitting gegenüber beiden verwandten Runge-Kutta Verfahren. Der Vergleich mit einer quantenmechanischen numerisches Lösung, welche mit dem Programm Qprop errechnet wurde und einen obere Schranke für die Ionisationswahrscheinlichkeit lieferte, konnte die Ergebnisse mit der klassischen Näherung nicht vollständig verifizieren. Jedoch sind die aufgetretenen Probleme bekannt und sind nicht mit dem Strang-splitting in Verbindung zu bringen. Zusammengefasst konnte die sehr ermutigende Leistungsfähigkeit des Strang-splittings, ausgelöst durch seine Eigenschaften (Symplektizität, Symmetrieerhaltung, Zeitumkehrbarkeitserhaltung and Erhaltung von Invarianten erster Ordnung), erfolgreich demonstriert werden und weitere Forschungsmöglichkeiten wur-

den vorgeschlagen.

Contents

1 Introduction

Quantum Mechanics is able to analytically predict all stationary states of the hydrogen atom along with its time evolution. Furthermore hydrogen-like atoms or hydrogen-like ions (i.e. systems with a number Z of protons and one valence electron) are also described by that model. A sufficient induced rise in the energy of the electron can result in its ionisation prompting the escape of the electron. The most popular experimental technique applied to bring about this process is the radiation exposure of the atom. Especially electromagnetic radiation emitted by lasers is used. As described in [1] current lasers can reach intensities more than high enough to reach ionisation for hydrogen atoms and hydrogen-like atoms/ions. Furthermore [2] mentions that it is experimentally challenging to determine the intensity of these ultra-strong lasers. An approach is to use the ionisation processes in the form of the determination of the ionisation probability of multiply charged ions. Many experimental techniques have been employed to achieve measurements. Full control of all parameters of the lasers is needed to bring them to proper use in engineering and science. Additionally the creation of fitting designs and a proper understanding of all interactions demand a theoretical formalism enabling simulations of these systems to predict key features, such as the dependence of the ionisation probability of such an atom/ion on the laser intensity, in advance computationally. Depending on the intensity and the type of atom/ion considered non-relativistic or relativistic quantum mechanics is the theoretical framework to be used on the current scientific level of knowledge.

The Dirac and the Schrödinger equations are the two equations of which either one can be chosen to be describe the interaction processes of atoms and ions in strong laser fields(Relativistic or non-relativistic treatment). It is in general not possible to find an analytic solution to most of these systems. Consequently an approximate analytical or numerical solution of these system has to be performed to achieve theoretical physical insight. Rigorous quantum mechanical solutions derived from the Schrödinger or the Dirac equation are very challenging with respect to computational resources needed. Thus there are a number of classical approaches(often simulating quantum mechanical behaviour) to treat these systems. Consequently this thesis will deal with one of these techniques in form of the classical Monte Carlo method as suggested by Abrines and Percival in [3, 4]. In this method the quantum mechanical states are replaced by ensembles of non-interacting classical particles mimicking quantum mechanical behaviour by considering averages over enormous numbers of trajectories. The treatment will be limited to the non-relativistic case in this thesis. It is hence important to stay within the non-relativistic regime.

This thesis' goal is to refine answers to the two fundamental questions arising in

that context:

- To what extent is the employed classical method describing the actual quantum mechanical dynamics?
- What methods need to be employed to solve the classical equations of motion numerically without numerical artefacts?

In [5] Heiko Bauke et al. have already performed some of this analysis in respect to a comparison between quantum mechanical and classical ionisation of hydrogen-like atoms in strong laser fields. However, the analysis was only conducted on one- and two-dimensional model systems with soft-core potentials. Hence, this thesis will expand these investigations to three-dimensional model systems using the dipole approximation as presented for example in [6]. The numerical solution of the classical equations of motion in this context mainly involves a solution to the classical Kepler problem. Standard integrators can produce numerical artefacts while solving this problem especially for trajectories that involve a low angular momentum. These artefacts are caused by high velocities that the considered orbiting particle encounters in trajectory points close to the core it is orbiting. Consequently this is resulting in an inaccurate rendering of the trajectory by most standard integrators with unadaptive time-steps. Therefore an artificial gain in energy is induced culminating in entirely different dynamics not caused by physical but by numerical effects.

As a remedy to these problems a method described in [7] by Balaraman and Vrinceanu will be employed involving a (classical) split-operator method. The Hamiltonian function resulting from a particle in a combined Coulomb (Kepler) and a laser is split into the analytically solvable pure Kepler part and the analytically or numerically solvable laser field-induced external field. Therefore, the solution should not be influenced by the low angular momenta problem encountered by many standard integrators as the Kepler problem is solved analytically in every time-step. Moreover, the laser field may be replaced by any perturbation possible which does not necessarily need to be small compared to the Kepler part of the problem. Depending on the perturbation an analytical solution of the perturbation may also be possible in some cases. Accordingly the numerical artefacts should be much lower for this method than with standard integrators such as the Runge-Kutta method. This thesis will employ the Runge-Kutta method as a point of comparison as it is a widespread scheme and hence data is available for comparison. Also the performance of the schemes is well known. In order to achieve a suitable comparison and investigate the quality of the mimicking of quantum mechanical behaviour as well as the numerical solution's, two additional simulations involving the same problems will be carried out. Following this train of thought a Runge-Kutta integration of the classical equations of motion will be executed as well as a quantum-mechanical simulation using the program *Qprop* as presented in [8].

2 Theoretical formalisms used to describe ionisaiton processes in hydrogen-like atoms or hydrogen-like ions

Initially the theoretical concepts that were utilised in this thesis will be briefly presented in the following. The first subsection will deal with the general description of ionisation processes in classical mechanics and quantum mechanics. Secondly, the process and schemes used to create ensembles of non-interacting particles and to propagate them in laser fields will be characterised. Lastly, a brief introduction of the numerical schemes and techniques used will be given to complete the picture.

2.1 Quantum mechanical treatment

2.1.1 Basic equations of motion

In non-relativistic quantum mechanics the Schrödinger equation is the equation governing the dynamics any system. Its time dependent form is

$$i\hbar\frac{\partial}{\partial t}\left|\psi\right\rangle = \hat{H}\left|\psi\right\rangle, \tag{2.1}$$

where $\hat{H}$ is the Hamilton operator of the system and $|\psi\rangle$ is the quantum state of the system. This equation applies in all situations without exception. If only one particle is considered the Hamiltonian is

$$\hat{H} = \frac{(\hat{\boldsymbol{p}} - q\hat{\boldsymbol{A}})^2}{2m} + q\hat{\Phi}, \tag{2.2}$$

where $\hat{\boldsymbol{p}}$ is the momentum operator, $\hat{\boldsymbol{A}}$ is an arbitrary vector potential, $\boldsymbol{\Phi}$ is an arbitrary scalar potential, m is the mass of the particle and q is the charge of the particle. In the case that real space is used as a Hilbertspace the momentum operator is represented by $-i\hbar\nabla$ and hence the Hamiltonian becomes

$$\hat{H} = \frac{(-i\hbar\nabla - q\boldsymbol{A}(\boldsymbol{r},t))^2}{2m} + q\Phi(\boldsymbol{r},t). \tag{2.3}$$

2.1.2 Ionisation in strong Laser fields

A hydrogen-like atom or ion of charge Z is considered which consists of a nucleus of charge Ze (e is the elemental charge) and a valence electron. The other electron shells

are either non-existent or totally closed and hence are assumed to not contribute sufficiently enough to the dynamics to be treated as well. If the pure atom is considered one has a two particle Hamiltonian of the form

$$\hat{H} = -\frac{\hbar^2}{2m_\mathrm{e}}\Delta_\mathrm{e} - \frac{\hbar^2}{2m_\mathrm{nucleus}}\Delta_\mathrm{nucleus} - \frac{Ze^2}{4\pi\epsilon_0|\boldsymbol{r}_\mathrm{e} - \boldsymbol{r}_\mathrm{nucleus}|}. \tag{2.4}$$

where ϵ_0 is the dielectric constant of the vacuum (when vacuum is considered what is assumed in this thesis) and $\boldsymbol{r}$ denotes the position vectors of the nucleus and the valence electron respectively. Because the mass of an electron is 1836 times smaller than the mass of a proton it can surely be assumed that the nucleus will almost be stationary compared to the electron. Hence the Born-Oppenheimer approximation is used for the nucleus in which it is considered to be stationary and is placed fixed at the origin of the system. In the case of an hydrogen atom it is possible to use the reduced mass to account for the actually non-fixed nucleus. However the contribution is small and it is more generally possible to treat problems. Consequently the Hamiltonian transforms to

$$\hat{H} = -\frac{\hbar^2}{2m_\mathrm{e}}\Delta_\mathrm{e} - \frac{Ze^2}{4\pi\epsilon_0|\boldsymbol{r}_e|}. \tag{2.5}$$

To model ionisations the external laser field needs to be included into the calculation. This requires the inclusion of both the scalar potential Φ and the vector potential $\boldsymbol{A}$ corresponding to the electromagnetic wave into the calculation as a potential and a canonic momentum respectively resulting in the Hamiltonian

$$\hat{H} = \frac{(-i\hbar\nabla + e\boldsymbol{A}(\boldsymbol{r}_\mathrm{e}, t))^2}{2m_\mathrm{e}} - \frac{Ze^2}{4\pi\epsilon_0\,|\,\boldsymbol{r}_\mathrm{e}\,|} - e\phi(\boldsymbol{r}_\mathrm{e}, t). \tag{2.6}$$

However, in this thesis the so called dipole approximation will be employed. A good summary of this method can be found in [6]. The method replaces the interaction of the electromagnetic wave with the atom by the interaction of the atom with a scalar potential at the origin $\phi = -\boldsymbol{E}(0,t)\cdot\boldsymbol{r}$ where $\boldsymbol{E}(0,t)$ is the electromagnetic field of the laser used. The vector potential is $\boldsymbol{A} = 0$ in this approximation. Consequently effects of the magnetic field are neglected as well as relativistic effects. As determined by Reiss in [9] it is not necessary to lift the entirety of the dipole approximation for more intense laser fields and/or shorter wavelengths. The result is that there is a regime were only the magnetic field needs to be included, but not the relativistic effects which begin in a regime with even higher intensity and/or shorter wavelength. The Hamiltonian thus reduces to

$$\hat{H} = -\frac{\hbar^2}{2m_\mathrm{e}}\Delta_\mathrm{e} - \frac{Ze^2}{4\pi\epsilon_0|\boldsymbol{r}_\mathrm{e}|} + e\boldsymbol{E}(0,t)\cdot\boldsymbol{r}_\mathrm{e}\,. \tag{2.7}$$

2.1.3 How can the ionisation probability be derived from a quantum mechanical state?

It is not trivial to determine the ionisation probability of electron(s) in an atom or ion even if its quantum mechanical state, a wavefunction in the case of a real space,

is known. Unlike in the classical case it is not valid, just to look at the total energy of the particle. The wavefunction will always have some bound amount and will hence yield a non-zero probability to find the electron in the atom as everywhere else in the universe. Consequently the energy is not a reliable criterion as a high ionisaiton probability might also be present when the particle still has a quantum mechanically negative energy.

One possibility to get results is the determination of the probability not to find the electron in any bound state

$$p_{\text{ion}} = 1 - \sum_{n=1}^{\infty} \sum_{l=0}^{n-1} \sum_{m=-l}^{l} \left\langle \psi_f \,\middle|\, \psi_{nlm} \right\rangle \ , \tag{2.8}$$

where $|\psi_f\rangle$ is the final wavefunction and $|\psi_{nlm}\rangle$ is a quantum state corresponding to a bound state determined by its three quantum numbers. Of course it is not possible to determine this infinite sum and a cut-off point must be chosen. The higher the order of the cut that has to be done on the principal quantum number n, the more precise the ionisation probability is determined.

Furthermore, it is possible to choose a different approach to the problem. One can define a sphere with Radius R around the nucleus that establishes a border between the atomic system and the outside world. Following this process the probability the final wavefunction will yield outside of this sphere

$$p_{\text{outside}} = \left\langle \psi_f(r > R) \,\middle|\, \psi_f(r > R) \right\rangle = 1 - \left\langle \psi_f(r \leq R) \,\middle|\, \psi_f(r \leq R) \right\rangle \tag{2.9}$$

can be calculated and is an approximation to the ionisation probability p_{ion}. The most serious problem of this scheme is the choice of R as quantum mechanics does not give a proper border of an atom. One could choose a value higher than the expectation value of the absolute value of the position vector corresponding to some excited state or take a point were the ground-state wavefunction or any bound state wavefunction will yield a probability below a certain value. Hence, it becomes evident that many reasonable choices for R are possible that will, however, produce different results.

2.2 Classical treatment

Abrines and Percival suggested and theoretically described a classical approximation to quantum mechanical ionisation processes in hydrogen or hydrogen-like atoms in [4]. The general concept is the replacement of the quantum mechanical expectation values by the average of the corresponding classical property calculated from a microcanonical ensemble of non-interacting classical particles.

The starting point of the classical description is the Hamiltonian function $\mathcal{H}_i(\boldsymbol{r_i}, \boldsymbol{p_i}, t)$ representing the total energy of the ith particle in the system where $\boldsymbol{r_i}$ is the generalised space coordinate, $\boldsymbol{p_i}$ is the corresponding canonical momentum and t is the

time. The Hamiltonian formalism yields the equations of motion for the system

$$\dot{\boldsymbol{r}}_i = \frac{\partial \mathcal{H}}{\partial \boldsymbol{p}_i}, \quad \dot{\boldsymbol{p}}_i = -\frac{\partial \mathcal{H}}{\partial \boldsymbol{r}_i} \tag{2.10}$$

from the Hamilton function. These equations exist for every particle (i.e. i times) and the vectorial description is to be understood as equations of motion for every component of the two canonical vectors $\boldsymbol{r}_i$ and $\boldsymbol{p}_i$.

2.2.1 Concrete equations for an atom/ion in a strong laser field

The hydrogen-atom/hydrogen-like ion is characterised by the Keplerian two body problem. Hence the convenient choice of a representation of the system via a center of mass system using the reduced mass μ and the relative distance of the two particles $\boldsymbol{r}$ is used. For additional convenience the center of the coordinate system is chosen to be the center of mass in whose gravitational field the other mass is moving.

Again the dipole approximation will be used in order to model the effect of the laser beam on the atom/ion. This results in the Hamilton function

$$H(\boldsymbol{r}, \boldsymbol{p}) = \frac{\boldsymbol{p}^2}{2\mu} - \frac{\alpha}{|\boldsymbol{r}|} + e\boldsymbol{E}(0,t) \cdot \boldsymbol{r} \tag{2.11}$$

for the system considered. Hence the differential equations

$$\dot{\boldsymbol{r}} = \frac{1}{\mu}\boldsymbol{p} \qquad \dot{\boldsymbol{p}} = -\alpha \frac{\boldsymbol{r}}{|\boldsymbol{r}|^3} - e\boldsymbol{E} \tag{2.12}$$

govern the dynamics of the system. As an analytical solution is in general not possible numerical methods will be used.

2.2.2 Preparation of the initial state

Before the propagation the initial conditions for the classical particles in bound states of the Kepler potential need to be determined. Abrines and Percival demand a microcanonical ensemble from which the initial conditions are uniformly sampled from. Additionally they mention that this induces the condition that the initial parameters determining the initial values need to be equally distributed on the 6 dimensional object in phase space which the microcanonical ensemble forms. A great simplification for spherically symmetric problems such as the Kepler problem is that in this case the Hamiltonian function is stationary and spherically symmetric in phase space as well. In [4] Abrines and Percival in detail describe the resulting energy and momentum distribution induced in a microcanonical ensemble. Moreover they deduce the uniform distribution of several quantities in this ensemble in the case of a spherically symmetric potential thus proving that one can create a microcanonical ensemble by uniformly distributing these parameters. Their efforts give rise to an algorithm to sample initial conditions where a uniformly distributed square of the angular momentum $\boldsymbol{L}^2$ is chosen as a basis.

The algorithm works as follows:

- Sample a $\boldsymbol{L}^2$ uniformly from the interval $(0, L^2_{\text{max}})$ where $\boldsymbol{L}^2_{\text{max}}$ is the highest possible value for the chosen energy
- Determine the point of closest approach (perihelion) for that $\boldsymbol{L}^2$
- Translate this state in time by an amount uniformly sampled from the interval $(0, T)$ where T is one period length corresponding to the E and $\boldsymbol{L}^2$
- Rotate the state in space via $R(\phi, \theta, \psi)$ in the Euler angle succession where ϕ, θ and ψ are sampled uniformly from the interval $(0, 2\pi)$

After running this algorithm all particles sampled form a valid microcanonical ensemble which can be used to mimic quantum mechanical behaviour when a large number of particles is sampled and averages of quantities are used to determine properties.

2.3 Numerical methods employed

As an analytical solution is not possible for the problem considered, a range of numerical methods will be employed and compared. Usually each method has certain advantages and disadvantages depending on the problem to be solved. The main goal is to have as little numerical artefacts as possible along with an accurate solution with as little need of computational power as possible. Whereas some methods are all-purpose methods, some are only applicable in certain cases and require certain forms of the differential equations or e.g. the potentials involved. Hence the three methods used in this thesis will be described in the following subsections.

2.3.1 Runge-Kutta method

This is one of the most famous numerical techniques used to solve ordinary differential equations of the form

$$\frac{d\boldsymbol{x}(t)}{dt} = \boldsymbol{f}(\boldsymbol{x}, t), \qquad \boldsymbol{x}(t_0) = \boldsymbol{x_0}, \tag{2.13}$$

where $\boldsymbol{x_0}$ is the initial value of the (possibly vector valued) searched function $\boldsymbol{x}(t)$ as presented in [10] which is the basis for this entire subsection. The general form of any Runge-Kutta scheme is

$$\boldsymbol{k_i}(x, t) = f(\boldsymbol{x_0} + h \sum_{j=1}^{s} a_{ij} \boldsymbol{k_j}, t_0 + c_i h) \tag{2.14}$$

$$\boldsymbol{x}(t + h) = \boldsymbol{x_0} + h \sum_{i=1}^{s} b_i \boldsymbol{k_i}\,, \tag{2.15}$$

where h is the step size and a_{ij}, b_i as well as c_i are sets of real constants. The Hamiltonian equations of motion are obviously of this form and consequently the Runge-Kutta method can be applied to the classical problem to be solved. Generally speaking the Runge-Kutta method is a finite difference method acting iteratively on a grid with certain combinations of forward and backward techniques. The estimation of the error in each step is the name-giving feature of each Runge-Kutta method. Within the Runge-Kutta method two approaches are known: The *explicit* schemes involve the direct calculation of the constants k_i in the system and the *implicit* scheme contains an iterative calculation of those. [10](page 192) derives a condition under which Runge-Kutta methods are *symplectic* i.e. they conserve the phase space volume. Furthermore, it becomes evident that only implicit Runge-Kutta schemes can be symplectic. An implicit Runge-Kutta scheme known to be symplectic usually produce results excelling in long time stability and a more exact conservation of energy because of the conservation of the phase space volume. In these cases they are known to be advantageous over explicit schemes which can never be symplectic. However the computational workload associated with them is known to be a bit higher. Runge-Kutta integrators are known to suffer from numeric artefacts originating in problems associated with high velocities of particles considered (e.g. Keplerian orbits at points close to the force center). This induces an artificial gain of energy. Moderately sized unadaptive time-steps are not able to properly render the higher velocity and the particle will non-physically gain energy. Some implicit Runge-Kutta integrators are not as prone to the problem because of their symplectic nature. Adaptive time-steps also partially solve the problem. Regrettably implicit Runge-Kutta schemes lose part of their symplectic nature when adaptive time-steps are used. However, these problems do not contribute much to the error in most cases (see e.g. [10] and [11]).

In the specific case of this thesis a symplectic implicit and an explicit 3rd order Runge-Kutta scheme will be used i.e. the error in each step is of the order of $O(h^4)$

where h is the step size. The scheme coefficients and calculation formulas are

$$\boldsymbol{k_1} = f\left(\boldsymbol{x} + \frac{5}{36}h\boldsymbol{k_1} + \frac{2}{9-\sqrt{15}/15}h\boldsymbol{k_2} + \frac{5}{36-\sqrt{15}/24}h\boldsymbol{k_3}, t + \frac{1}{2-\sqrt{15}/10}h\right) \tag{2.16}$$

$$\boldsymbol{k_2} = f\left(\boldsymbol{x} + \frac{5}{36+\sqrt{15}/24}h\boldsymbol{k_1} + \frac{2}{9}h\boldsymbol{k_2} + h\frac{5}{36-\sqrt{15}/24}\boldsymbol{k_3}, t + 0.5h\right) \tag{2.17}$$

$$\boldsymbol{k_3} = f\left(\boldsymbol{x} + \frac{5}{36+\sqrt{15}/30}h\boldsymbol{k_1} + \frac{2}{9+\sqrt{15}/15}h\boldsymbol{k_2} + h\frac{5}{36}\boldsymbol{k_3}, t + \frac{1}{2+\sqrt{15}/10}h\right) \tag{2.18}$$

$$\boldsymbol{x}(t+h) = \boldsymbol{x}(t) + \frac{5}{18}h\boldsymbol{k_1} + \frac{4}{9}h\boldsymbol{k_2} + \frac{5}{18}h\boldsymbol{k_3} \tag{2.19}$$

for the implicit scheme and

$$\boldsymbol{k_1} = hf(\boldsymbol{x}, t) \tag{2.20}$$

$$\boldsymbol{k_2} = hf\left(\boldsymbol{x} + \frac{\boldsymbol{k_1}}{2}, t + \frac{h}{2}\right) \tag{2.21}$$

$$\boldsymbol{k_3} = hf\left(\boldsymbol{x} - \boldsymbol{k_1} + 2\boldsymbol{k_2}, t + \frac{h}{2}\right) \tag{2.22}$$

$$\boldsymbol{x}(t+h) = \boldsymbol{x}(t) + \frac{\boldsymbol{k_1} + \boldsymbol{k_3}}{6} + \frac{2}{3}\boldsymbol{k_2} \tag{2.23}$$

for the explicit scheme,

where t is the time where the current time the propagation is at. The coefficients for the implicit scheme display the implicit nature of the scheme as the coefficients to be calculated are needed in its calculation. Hence initial guesses and an iterative solution are required.

2.3.2 Split-Operator

Split operator methods are widely employed in quantum mechanics and separate the Hamilton operator in to two(or more) parts. In this thesis this technique will be used on the Hamiltonian function of a classical system i.e. not the Hamilton operator, but the Hamiltonian function is treated. This subsection is primarily based on the outline presented in [7]. This description is inherently classical, however it is easily possible to transfer some arguments to quantum mechanics. The basis of all these schemes is the separability of the Hamiltonian function i.e.

$$H(\boldsymbol{r}, \boldsymbol{p}, t) = H_0(\boldsymbol{r}, \boldsymbol{p}, t) + H_1(\boldsymbol{r}, \boldsymbol{p}, t), \tag{2.24}$$

where $H(\boldsymbol{r}, \boldsymbol{p}, t)$ is the full scale Hamiltonian function of the system, $H_0(\boldsymbol{r}, \boldsymbol{p}, t)$ is one (usually this is aspired to be analytically solvable) part of the separable sum of the full scale Hamiltonian and $H_1(\boldsymbol{r}, \boldsymbol{p}, t)$ is another part of the separable sum. $\boldsymbol{r}, \boldsymbol{p}$ denote the general position and momentum coordinates and t denotes the time. In

classical mechanics the time-evolution of a function $\boldsymbol{z}(\boldsymbol{r},\boldsymbol{p},t)$ defined over the phase space is determined by its Poisson bracket with the Hamiltonian function

$$\frac{\mathrm{d}\boldsymbol{z}(\boldsymbol{r},\boldsymbol{p},t)}{\mathrm{d}t} = \{\boldsymbol{z}(\boldsymbol{r},\boldsymbol{p},t), H(\boldsymbol{x},\boldsymbol{p},t)\} := D_H \,, \tag{2.25}$$

where $\{,\}$ denotes the Poisson bracket. If a proper set of initial conditions $\boldsymbol{z_0} := \boldsymbol{z}(\boldsymbol{r_0},\boldsymbol{p_0},t_0)$ is given the trajectory of $\boldsymbol{z}(\boldsymbol{r},\boldsymbol{p},t)$ can be expressed as

$$\boldsymbol{z}(\boldsymbol{r},\boldsymbol{p},t) = e^{\Delta t D_H}\boldsymbol{z_0}, \tag{2.26}$$

where $\Delta t = t - t_0$. $e^{\Delta t D_H}$ suggests a connection to the quantum mechanical time-evolution operator of the Schrödinger picture. In case the mapping is known this can be expressed analytically and, hence, the trajectory can be determined. In the case of an separable Hamiltonian function the mapping can be expressed as

$$\boldsymbol{z} = e^{\Delta t(D_{H_0}+D_{H_1})}\boldsymbol{z_0}. \tag{2.27}$$

As both D_{H_0} and D_{H_1} are not simple numbers it is not trivially possible to separate the exponential function into a product of two exponential functions because the commutator $[D_{H_0}, D_{H_1}]$ is not necessarily 0. The Baker-Campbell-Hausdorff formula allows an expansion of the exponential function involving the commutators. However, a simple decomposition is not in general suitable for numerical calculations. The easiest known integrator with numerically favourable properties is the so called *Strang-splitting* which uses the approximation

$$e^{\Delta t(D_{H_0}+D_{H_1})} = e^{\Delta t D_{H_1}/2} e^{\Delta t D_{H_0}} e^{\Delta t D_{H_1}/2} + O(\Delta t^3) \tag{2.28}$$

$$= e^{\Delta t D_{H_0}/2} e^{\Delta t D_{H_1}} e^{\Delta t D_{H_0}/2} + O(\Delta t^3)\,. \tag{2.29}$$

The error of $O(\Delta t^3)$ can be derived from the expansion as shown in [7] and [10] page 86f. The factors of $1/2$ represent coefficients originating from the expansion. Furthermore an estimation of the integrals shown in [12] in equation (33.22) will lead to a similar result. One can easily convince oneself that this is true in many other pieces of literature or via a series expansion of the Strang-splitting. The expansion assumes a small time step, hence care must be taken not to use step sizes too large. Balaraman's and Vrinceanu's paper, in reference to [10], states the favourable properties of this integrator. It is known the be symplectic, symmetry preserving, time reversibility preserving and first-oder invariant preserving. All these properties are very favourable in long-time integration and should permit one to use it for the propagation of hydrogenlike atoms in laser fields.

In the case of hydrogenlike atoms/ions in strong laser fields using the dipole approximation the splitting results in

$$D_{H_0} = \frac{\boldsymbol{p}^2}{2m} - \frac{\alpha}{|\boldsymbol{r}|} \quad \text{called "Drift stage" as well as} \tag{2.30}$$

$$D_{H_1} = e\boldsymbol{E}(t)\cdot\boldsymbol{r} \quad \text{called "Kick stage"}\,, \tag{2.31}$$

where α is the Coulomb law constant(could also be any arbitrary 1/r potential constant for different problems), e is the elementary charge and $\boldsymbol{E}(t) = E_{\max} \sin \omega_l t$ (ω_l angular frequency of monochromatic laser) is the time-dependent electrical field strength of the laser used. In this thesis a field solely in the x-direction was considered to avoid calculation time becoming too large. This is a simple transformation and does not change the physics. Furthermore first variant, shown in (2.29), of the two equivalent ways of splitting is used as the Kepler stage is computationally more expensive than the laser stage. There are many more higher order integrators of this class which involve combinations of several Drift and Kick stages. [7] states several of these and their expansion coefficients. Generally their error is smaller, but not every combination is possible and not every valid combination has all desired favourable properties.

In the special case of hydrogenlike atoms/ions in a strong laser field in dipole approximation we can always analytically solve both the Drift stage as well as the Kick stage. Epsecially for the Keplerian part this is favourable as many standard integrators such as the Runge-Kutta scheme tend to produce numercial artefacts when solving this problem. This will furthermore boost the precision as no additional errors from numerical methods used in the two stages will contribute to the total error.

2.3.3 Methods for drift and kick stages of the split operator scheme

The Split operator method demands a numerical or analytic solution to the "drift" and "kick" stages. In the case considered here is an hydrogen atom in a laser potential in dipole approximation. The classical Kepler problem consequently acts as a drift and the scalar potential of a laser in dipole approximation acts as kick stage. Hence both of them can be propagated analytically in this case. As easy as it seems the drift stage actually needs an elaborate approach as it is the most time-consuming part of the calculation as shown by Balaraman and Vrinceanu. To avoid floating point calculations (for performance and precision reasons) and give an easier overview atomic units will be used thoroughly in this subsection.

Analytical solving method for the classical Kepler problem

The system is considered (as described before) in a center of mass system. The input vector is the state vector containing the current (relative) positions and momenta of the electron. The conserved quantities Energy E and the Runge-Lenz vector $\boldsymbol{A}$ ($\boldsymbol{A}$ in this subsubsection describes the Runge-Lenz vector, not the vector potential) can be kept (along with the angular momentum vector $\boldsymbol{L}$ of which the absolute value is conserved) in the status vector to save calculation time. If they are not in the state vector they will have to be computed at this point as an efficient algorithm to analytically propagate the problem will make use of all conserved quantities. This is subsection is based on the paper of Balaraman and Vrinceau along with own calculations for the hyperbolic case. The parabolic case was treated as described in [13].

In a first step the conserved quantities are calculated, if necessary, following the equations

$$E_0 = \frac{\boldsymbol{p}^2}{2\mu} - \frac{\alpha}{|\boldsymbol{r}|} \tag{2.32}$$

$$\boldsymbol{L} = \boldsymbol{r} \times \boldsymbol{p} \tag{2.33}$$

$$\boldsymbol{A} = \boldsymbol{p} \times \boldsymbol{L} - \mu\alpha\boldsymbol{e}_r. \tag{2.34}$$

Additionally the eccentricity given by $\epsilon = \frac{|\boldsymbol{A}|}{\alpha\mu}$ is computed to determine the type of classical Kepler orbit.

$$Orbit = \begin{cases} \text{Circle}, & \text{if } \epsilon = 0 \\ \text{Ellipsis}, & \text{if } \epsilon < 1 \\ \text{Parabola}, & \text{if } \epsilon = 1 \\ \text{Hyperbola}, & \text{if } \epsilon > 1 \end{cases} \tag{2.35}$$

These cases could also be divided by using the energy. As needed in all cases the angular orbital frequency is calculated to $\omega = \left(\frac{2|E|}{m}\right)^{3/2} \frac{1}{\alpha}$.

$\epsilon = 0$ In the circle case the absolute value of the position and momentum vector are constant. Hence the position and momentum vector are rotated $\omega\Delta t$ around the angular momentum axis. This case is neccessary as the ellipsoid case involves the eccentricity in a denominator and hence would produce singularties.

$\epsilon \neq 0$ Because of the fact that they are needed and properly defined in all following cases the semi-major axis $a = \frac{\alpha}{2E}$, the direction of the pericenter $e_1 = \frac{\boldsymbol{A}}{\epsilon}$ and the orbital plane perpendicular to it $e_2 = \frac{\boldsymbol{L}\times\boldsymbol{A}}{\epsilon|\boldsymbol{L}|}$ are calculated.

$0 < \epsilon < 1$ Initially here we need the eccentric elliptic anomaly of the initial position $u_0 = \arctan(1 + 2E, \sqrt{\frac{-2E}{\mu}}\boldsymbol{r} \cdot \boldsymbol{L})$. In the following the transcendent Kepler's equation $\text{Kepler}(\epsilon, M) : u - \epsilon \sin u - M = 0$ for the advanced time is solved numerically for the later time i.e. $\text{Kepler}(\epsilon, u_0 - \epsilon \sin u_0 + \omega\Delta t)$. As a normal fixed point iteration involved problems Halley's method, as presented in [14], was used to numerically solve the equation. After that the positions and momenta are updated via

$$\boldsymbol{r} = a(\cos u - \epsilon)\boldsymbol{e_1} + a\sqrt{1-\epsilon^2}\sin u\boldsymbol{e_2} \tag{2.36}$$

$$\boldsymbol{p} = -\sqrt{\frac{\alpha m}{a}}\frac{\sin u}{1-\epsilon\cos u}\boldsymbol{e_1} + \sqrt{\frac{\alpha\mu - \epsilon^2}{a}}\frac{\cos u}{1-\epsilon\cos u}\boldsymbol{e_2}. \tag{2.37}$$

$\epsilon = 1$ This is the parabolic case. As it was difficult to transfer the scheme used before, a scheme from a paper by Condurache and Martinui [13] was used. This

paper uses a rescaled time $\tau(t)$. As we here update momentum and position the v was replaced by $\frac{p}{\mu}$, r_0 etc. denotes the value of the quantity before the time step Δt is performed. Initially this value must be obtained from the equation

$$\Delta t = |r_0|\tau(t) + \frac{\tau^2(t)}{2\mu}(r_0 \cdot p_0) + \alpha\frac{\tau^3(t)}{6\mu}. \tag{2.38}$$

Note that the paper incorrectly states 3 for the last coefficient. As iterative techniques such as the fixed point methods are prone to not converge for third order equations a technique to analytically solve third order equations from [15] was used. After that the update was performed following

$$r = r_0 + \tau(t)|r_0|\frac{p_0}{\mu} - \frac{A}{2\mu} \tag{2.39}$$

$$p = \frac{|r_0|p_0 - \tau(t)A}{|r|}. \tag{2.40}$$

$\epsilon > 1$ This is the Hyperbolic case which can be seen as analogous to the elliptic case. Most quantities initially calculated are involved in the equations. Likewise as before the initial hyperbolic eccentric anomaly $H_0 = \text{atanh}(\frac{|r_0|}{\epsilon|a|})$ is calculated. Then the hyperbolic Kepler's equation $\text{HKepler}(\epsilon, M) : e\sinh H - H - M = 0$ is solved for the advanced time $\text{HKepler}(\epsilon, \epsilon\sinh H_0 - H_0 + \omega\Delta t)$ using Halley's method, as presented in [14], again. Following that step again the updates are performed via

$$r = |a|(\epsilon - \cosh H)e_1 + |a|\sqrt{\epsilon^2 - 1}\sinh H e_2 \tag{2.41}$$

$$p = \mu\sqrt{\frac{\alpha m}{|a|}}\frac{\sinh H}{\epsilon\cosh H - 1}e_1 - \mu\sqrt{\frac{\epsilon^2 - 1}{a}\alpha\mu}\frac{\cosh H}{\epsilon\cosh H - 1}e_2. \tag{2.42}$$

It is imaginable that this algorithm will use lots of computational power. The process to find solutions to the transcendent equations along with the many calculations to be performed in the updates result in the high running time. .

Analytical solving method for the dipole laser potential

This section is mostly based on Balaraman and Vrinceanus's paper again.

If only the dipole approximation is used, only the momentum of the particle will change. The potential for an electron is given by $\phi = E \cdot r$. Furthermore a monochromatic laser with orbital frequency ω_l and peak electrical field strength $E_{\max}$ is assumed. The change is given by

$$p - p_0 = \int_{t_0}^{t_0+\Delta t} F\text{dt} = \int_{t_0}^{t_0+\Delta t} E_{\max}\sin\omega_l t\text{dt} = E_{\max}(-\cos\omega_l(t_0 + \Delta t) + \cos\omega_l(t_0). \tag{2.43}$$

This process will be much less computationally expensive than the Drift stage. This justifies the choice of the Strang-splitting method involving less Drift stages than Kick stages.

2.3.4 Determination of ionisation probability in the classical Monte Carlo method

In classical mechanics a particle orbiting a Keplerian potential is considered bound as long as its total energy is below zero. Thus a single particle trajectory can be considered ionised as soon as the total energy associated with it passes the border of zero. Consequently this analysis has to be performed on the final energies of the particle after propagation. As the Monte Carlo method employs ensembles of non-interacting particles the partition of particles ionised has to be determined. Hence the ionisation probability is given by

$$p_{\text{ion}} = \frac{n(E > 0)}{N} \,, \tag{2.44}$$

where $n(E > 0)$ is the number of particles from the current ensemble that have positive energy after propagation and N is the total number of particles (samples) in the current ensemble.

2.3.5 Qprop

Qprop is a program originally developed by Dieter Bauer as presented in [8] to numerically solve a set of quantum mechanical problems. The set consists of problems with spherically symmetric unperturbed systems of atoms/ions later exposed to laser fields in dipole approximation. This entire section will be heavily based on [8]. Additionally the focus will primarily be set on the parts of the program used for this thesis.

General description and numerical solution technique employed

As mentioned in the previous subsection (2.1) is the basic equation governing the (non-relativistic) dynamics of all quantum mechanical problems. The Hamilton operator for one particle is given by (2.2) if spin is ignored. For N particles the problem becomes tremendously complicated as a $3N$-dimensional Hilbertspace containing an N-dimensional state (a wavefunction in real space). As even a numerical solution of this problem requires more computational effort than reasonably available, several schemes have been developed(For example Hartree-Fock and Quantum Monte Carlo methods). The additional complication is that (especially in atomic or molecular systems) correlation interaction and Pauli exculsion principle need to be obeyed. Qprop employs a scheme called *Denstiy Function Theory* (DFT) in its time-depedent version (TDDFT). DFT uses the Hohenberg-Kohn theorem which states

that the ground state of any electron system is uniquely defined by the electron density $n(\boldsymbol{r}, t)$ which is only dependent on the three space coordinates and time, NOT on the number of particles N.

However in this thesis only the Hydrogen atom will be treated. Hence Density Functional Theory is not needed to perform the required task. Qprop is also able to solve the Time-Dependent Schrödinger equation via a imaginary and real time propagation technique that will be summarised in the following.

Real time propagation algorithm

Qprop employs the technique of propagators in order to propagate states (quantum mechanical states to be precise) in time. Equation (2.2) (implies the propagator

$$U(t_1, t_2) = T \exp\left(-i \int_{t_1}^{t_2} H(\tau) \mathrm{d}\tau\right) \tag{2.45}$$

where T is the time-ordering operator. Hence in the special cases treated in Qprop the wavefunctions evolve over time according to

$$\psi(\boldsymbol{r}, t_2) = U(t_2, t_1)\psi(\boldsymbol{r}, t_1) \tag{2.46}$$

As usual in numerics the time-propagation is realised via consecutive small time step evolution of size Δt. Consequently a possible time-dependence in time ordering and the possibly explicit time-dependence of the Hamiltonian can be ignored resulting in the short-time propagator

$$U(t + \Delta t, t) \approx \exp\left[-i\Delta t H(t + \Delta t/2)\right] \quad \text{implying an evolution from } t_0 \text{ to } t_f \tag{2.47}$$

$$\text{as} \quad U(t_f, t_0) = \prod_{i=0}^{M-1} U(t_i + \Delta t, t_i) \tag{2.48}$$

where $\Delta t = (t_f - t_0)/M$ (M is the total number of time steps performed). [8] contains a detailed description of the approximations and techniques used to achieve a diagonal and easily numerically treatable Hamiltonian including, e.g., the Crank-Nicoloson approximation. As the detailed formalism is not the point of this thesis Bauer's and Korval's paper is recommended to learn about that.

Imaginary time propagation

Qprop applies a propagation in imaginary time to determine the ground state of a quantum system. Only a fairly little number of potentials allow it to determine an analytical solution for the ground state of a system. Hence numerical techniques are used. In many cases the fact is used that the ground state's total energy is minimal in the system. Qprop employs the propagator used for real time propagation with the real time step replaced by an imaginary one i.e.

$$\Delta t \to -i\Delta t \,. \tag{2.49}$$

As in [8] an outline why this technique determines the ground state will be given.

An unperturbed quantum mechanical system with bound states is considered. Following the mathematics of Hilbert spaces an arbitrary quantum state $|\psi\rangle\,(t)$ can be expanded as

$$|\psi\rangle\,(t) = \sum_n a_n \exp(-i\epsilon_n t)\,|\psi_n\rangle\ , \tag{2.50}$$

where $a_n = \langle\psi_n\,|\,\psi(t)\rangle$ is the expansion coefficient, ϵ_n is the energy of the n-th bound state and $\exp(-i\epsilon_n t)$ is the time evolution operator $\exp(-i\hat{H})$ (where $\hat{H}$ is the Hamiltonian operator of the quantum system) in the Schrödinger picture inducing propagation in time which has acted on $|\psi_n\rangle$. Accordingly a propagation of one imaginary time step results in the relation

$$|\psi\rangle\,(\Delta t) = \sum_n a_n \exp(-i\epsilon_n \Delta t)\,|\psi_n\rangle\ , \tag{2.51}$$

where the initial time t_0 is implied to be $t_0 = 0$. The factor $\exp(-\epsilon_n \Delta t)$ has an extremal value for $\epsilon_n = \epsilon_0$ i.e. the ground state energy. This implies that the ground state decays slowest (if $\epsilon_0 > 0$) or blows up fastest (if $\epsilon_0 < 0$). As a result the renormalised $|\psi\rangle\,(t)$ converges to the ground state $|\psi_0\rangle$. Ergo any initial guess for a state converges that way. Note that the initial guess, of course, has an influence on the convergence rate, but [8] claims that the influence is not critical and that random choices are sufficient.

Hamiltonian for single electron atoms in linearly polarised laser fields

The Hamiltonian for a hydrogenlike atom/ion in a laser field is given by

$$H(t) = -\frac{1}{2}\Delta + V_I(t) \tag{2.52}$$

where $V_I(r)$ is the interaction with the laser field in dipole approximation and $V(r)$ is the central potential of the atom. The dipole approximation term is given as

$$V_I(t) = -\boldsymbol{A}(t)\frac{\partial}{\partial z} + \frac{\boldsymbol{A}^2}{2} + z\boldsymbol{E}(t) \tag{2.53}$$

where $\boldsymbol{A}$ is the vector potential (restricted to the z direction) and $\boldsymbol{E}(t)$ is the electric field of the laser. Either length gauge (only third term) or velocity gauge (only first two terms) can be used. Depending on the electric field amplitude, other parameters and the expected ionisation regime Qprop chooses one of the two, as one of them is always advantageous considering the computational cost needed. For example it is advantageous to treat heavy ions in length gauge, whereas it is more advantageous to treat higher-order above threshold ionisation in velocity gauge.

3 Numerical experiments

This chapter contains the results of the numerical experiments performed with the explicit and implicit Runge-Kutta schemes, the Split-Operator scheme as well as Qprop. The system considered will be a hydrogen atom in a monochromatic laser field in dipole approximation. It was aspired to achieve results for all schemes that can be compared with each other to properly rate their performance. It was taken care that the parameters used are in the regime where the dipole approximation and non-relativistic treatment are still valid (Information in Reiss' paper [9]). The exact experiment parameters and modi operandi for the evaluation will be presented in this chapter as well. Moreover initial comparisons will be performed and some conclusions will be derived.

3.1 Remarks on programs used

The Split-Operator method was implemented in a self-written C++ program whose source code can be provided on request. The Runge Kutta method uses a similar main program and the same algorithms to determine the starting positions as to be seen in its source code in the appendix. The Runge-Kutta integrators were taken from the *TADS* library composed by *Heiko Bauke* (For contact information see the paper [5]). The program Qprop was used as offered by *Dieter Bauer* (see [8]). More precisely the *hydrogen* example code was used and modified to fit the needs of these experiments.

3.2 Split-Operator vs. Runge-Kutta

3.2.1 Parameters for the classical system and integrators

This section contains the comparative numerical experiments on the hydrogen atom in the monochromatic laser field using the dipole aproximation. The first numerical experiments involved a test of the Split-Operator technique and an explicit and an implicit 3rd order Runge-Kutta scheme. The initial energy was chosen to $E_0 = -0.5$ a.u. and 100 000 samples were used. The laser wavelength was initially chosen to $\lambda = 3000$ a.u. ≈ 158 nm. The pulse duration was chosen to one full laser period $t_{\text{run}} = T_{\text{laser}}$. The peak electrical field strength E_{max} was varied bet ween 0.0 a.u. and 1.0 a.u in 50 steps. This is approximately 16 times as large as the ionisation suppression barrier. As this experiment also partially is a performance test, the step size was

varied to see differences in the performances of the different schemes. The main interest is the ionisation probability, hence only the energies were recorded and used to determine the number of ionised particles i.e. trajectories which end at $E > 0$. The simulation time was chosen to one laser period and the step size was varied from $\Delta t = 0.19635$ a.u. to $\Delta t = 0.000\,766\,99$ a.u. . The odd values of the step sizes originate from the fact that the step sizes are fractions of the unperturbed Kepler problems period.

3.2.2 Comparison of the preservation of the microcanonical ensemble for a deactivated laser field

In order to verify to what extend the numerical solutions preserve the microcanonical distribution initially created with a deactivated laser field histogram plots of the energy distributions of all numerical integrators for a deactivated laser field for different step sizes are plotted. The main goal is to determine to what extend the problem, that the Runge Kutta scheme has a unphysical gain of energy for low angular momenta trajectories when numerically solving the Kepler problem, influences the energy distribution. As the Split-operator scheme analytically solves the Kepler problem there should be only a spread of energies in the order of magnitude of the precision used. Ideally a microcanonical ensemble only contains particle of a single energy.

Figure 3.1 shows histogram results for the zero electric field amplitude and the largest step size. It becomes evident that the implicit as well as the explicit Runge-Kutta scheme show a large number of particles that have an enormous amount of energy during the pure Kepler propagation as to be seen in figures 3.1b and 3.1c. This must be related to numerical problems associated with low angular momenta in Keplerian potentials as a gain of that much energy is not physically possible given the parameters of the system. The implicit scheme has a slight advantage in comparison to the explicit scheme the amounts of energy gained by numerics is is smaller. Not the different scales in the figures. However, it becomes evident that Runge-Kutta schemes cannot properly integrate the system at such a large step size.

This error destroys the microcanonical distribution and makes the results unfit to imitate quantum mechanical behaviour. For this step size the Runge-Kutta schemes are usable to integrate the system without and consequently also with the laser field as the microcanonical ensemble is already disturbed by the artificial energy gain. In contrast to that the Split-Operator scheme shows a reasonable spread of energies. The energy mostly only differs in the order of magnitude of the precision used. This is to be expected as the Split-Operator method simply analytically solves the Kepler problem for $E_0 = 0$ a.u. and this must be independent of step size within error precision. For a step size roughly 2000 times smaller than the initial size the picture is not much different. The two Runge-Kutta schemes still have the numerical artefact of artificial energy gain as to be seen in figures 3.2b and 3.2c. The smaller step size lowered the number of such particles epsecially for the implicit Runge-Kutta integration of the Kepler propagation. The Strang-splitting performing the analytical solution

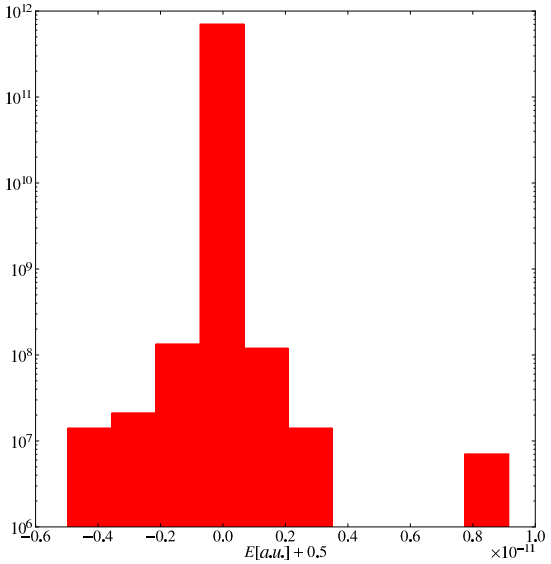

(a) Split Operator

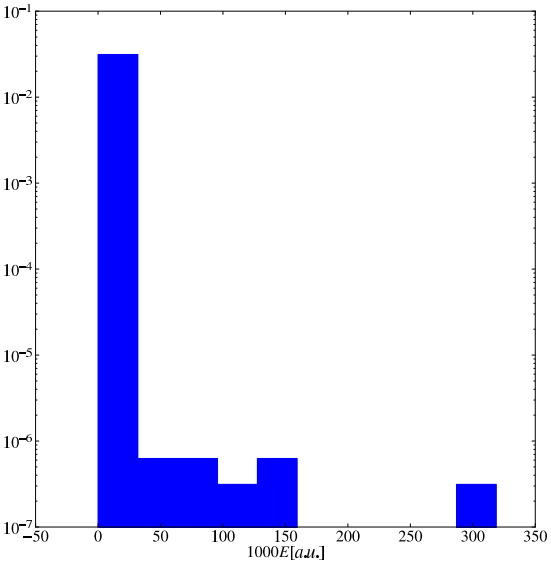

(b) Runge-Kutta, Implicit

Figure 3.1: Histogram of final energies for $E_{\max} = 0$ a.u. and step size $\Delta t = 0.196\,35$ a.u., wave length of laser $\lambda = 3000$ a.u., Initial energy $E_0 = -0.5$ a.u., 100 000 samples, Simulation time $t_{\text{run}} = T_{\text{laser}}$, CComparison between the Strang-splitting Split-Operator scheme and the implicit and explicit 3rd oder Runge-Kutta methods on a hydrogen atom in a monochromatic laser field using dipole approximation; Note the different scales of each diagram, especially the Split-Operator figure 3.1a

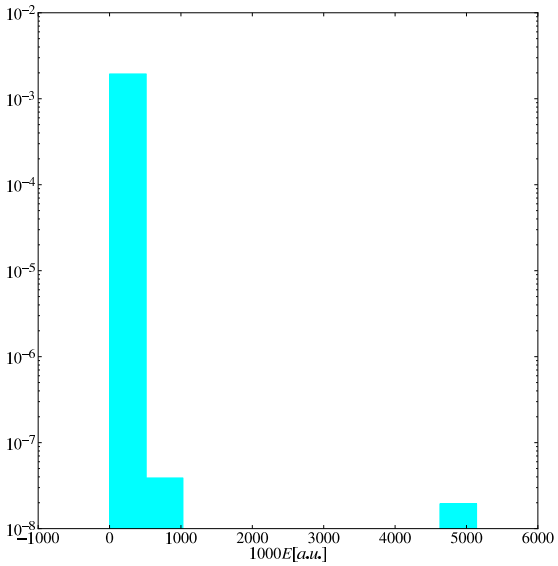

(c) Runge-Kutta, Explicit

Figure 3.1: Histogram of final energies for $E_{\max} = 0$ a.u. and step size $\Delta t = 0.196\,35$ a.u., wave length of laser $\lambda = 3000$ a.u., Initial energy $E_0 = -0.5$ a.u., 100 000 samples, Simulation time $t_{\text{run}} = T_{\text{laser}}$, Comparison between the Strang-splitting Split-Operator scheme and the implicit and explicit 3rd oder Runge-Kutta methods on a hydrogen atom in a monochromatic laser field using dipole approximation; Note the different scales of each diagram, especially the Split-Operator figure 3.1a

of the Kepler problem in this case generally shows the same picture as before in the form of a small spread of energies around the desired energy indicating the canonical nature of the ensemble. Additionally to the just mentioned fact figure 3.2a also displays that the spread has become a bit larger. Actually there should be no dependence on step size for numerical solutions, nevertheless even an analytical solution is still rendered in the limits of a computational system. Finite number representation and calculations with it (especially floating point calculations) always give rise to round of errors and truncation errors. A larger number of time-steps will induce this errors to accumulate. Figure 3.3 shows the same plots for the smallest step size used in this experiment. Again the picture is generally the same as for the other time steps. The smaller step size decreases the number of particles that artificially gain energy for numerical solution using the implicit and explicit Runge-Kutta scheme as to be seen in figures 3.3b and 3.3c. However, there is still a significant amount of these particles both for the implicit and explicit Runge-Kutta solution. There is little change for the Split-operator solution apart from a quite tiny increase of the spread related to finite number representation as to be investigated in figure 3.3a.

In summary the analysis of the histograms reveals that both 3rd order Runge-Kutta schemes fail to preserve the microcanonical ensemble without an activated laser field. Theoretically the energy should stay constant for a pure Keplerian potential over long periods of time. As the running time of the simulation is a full laser period the Runge-Kutta schemes develop the problematic artificial energy gain quite profusely as large numbers of Keplerian periods and the problems with low angular momenta trajectories are augmented each period which can for example be seen in [11]. For the initial energy $E_0 = -0.5$ a.u. and the laser wavelength $\lambda = 3000$ a.u. the running time of the simulation is to $t_{\text{run}} \approx 411\,000$ a.u. which is about 65 412 Keplerian orbits at the chosen energy. All this induces the artificial energy gain resulting in artificial ionisation of particles that will interfere with the actual ionisation probability. The Split-operator Strang-splitting produces very satisfactory results in this context as the problem is solved analytically. This avoids the problems that appeared with the Runge-Kutta schemes entirely as ionsation is really induced by the Kick stage of the Strang-splitting of the Split-operator method modeling the laser field. Consequently only the pure numerical errors estimated for the splitting will be present in the numerical calculation for a switched on laser field.

3.2.3 Results with activated laser field

Now the laser field is switched on according to the parameters mentioned at the start of this section. Initially the ionisation probability resulting for the three different numerical methods is determined and compared for different step sizes where the electrical field amplitude E_{max} was varied from 0 a.u. to 1.0 a.u.. Afterwards the energy distribution for $E_{\text{max}} = 0.5$ a.u. was analysed followed by a running time analysis of all schemes in order to test the computational performance of the programs and relate them to the quality of the results obtained.

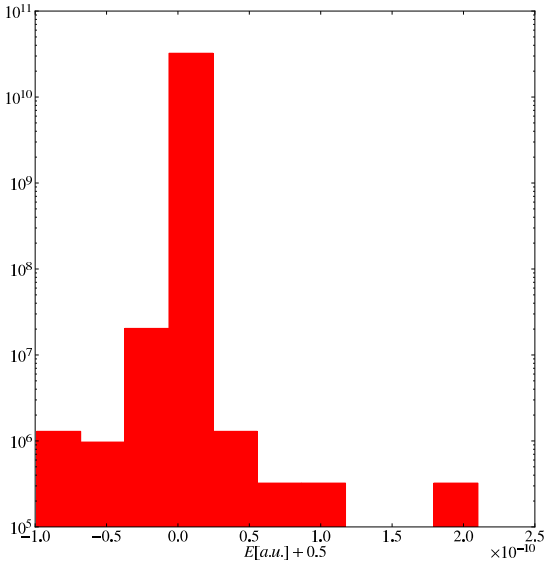

(a) Split Operator

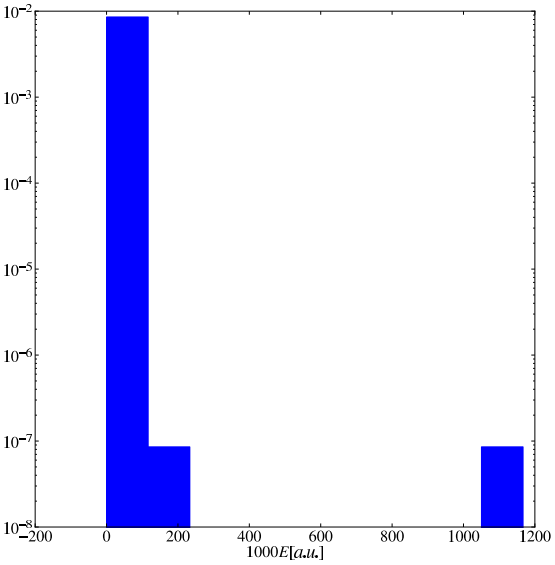

(b) Runge-Kutta, Implicit

Figure 3.2: Histogram of final energies for $E_{\max} = 0$ a.u. and step size $\Delta t = 0.003\,067\,96$ a.u., wave length of laser $\lambda = 3000$ a.u., Initial energy $E_0 = -0.5$ a.u., 100 000 samples, Simulation time $t_{\text{run}} = T_{\text{laser}}$, Comparison between the Strang-splitting Split-Operator scheme and the implicit and explicit 3rd oder Runge-Kutta methods on a hydrogen atom in a monochromatic laser field using dipole approximation; Note the different scales of each diagram, especially the Split-Operator figure 3.2a

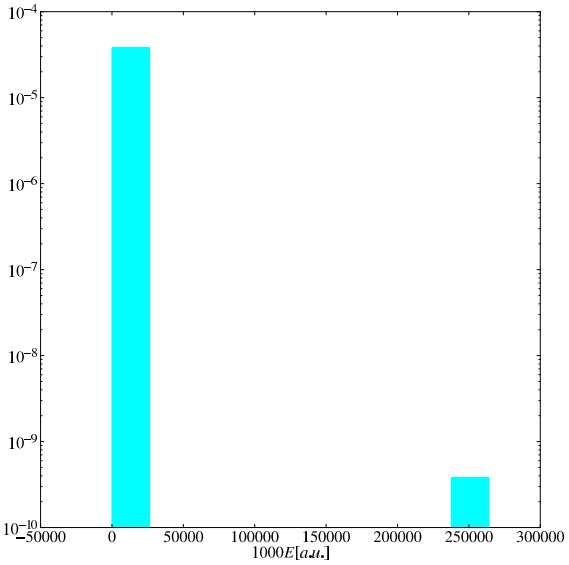

(c) Runge-Kutta, Explicit

Figure 3.2: Histogram of final energies for $E_{\max} = 0$ a.u. and step size $\Delta t = 0.003\,067\,96$ a.u., wave length of laser $\lambda = 3000$ a.u., Initial energy $E_0 = -0.5$ a.u., 100 000 samples, Simulation time $t_{\text{run}} = T_{\text{laser}}$, Comparison between the Strang-splitting Split-Operator scheme and the implicit and explicit 3rd oder Runge-Kutta methods on a hydrogen atom in a monochromatic laser field using dipole approximation; Note the different scales of each diagram, especially the Split-Operator figure 3.2a

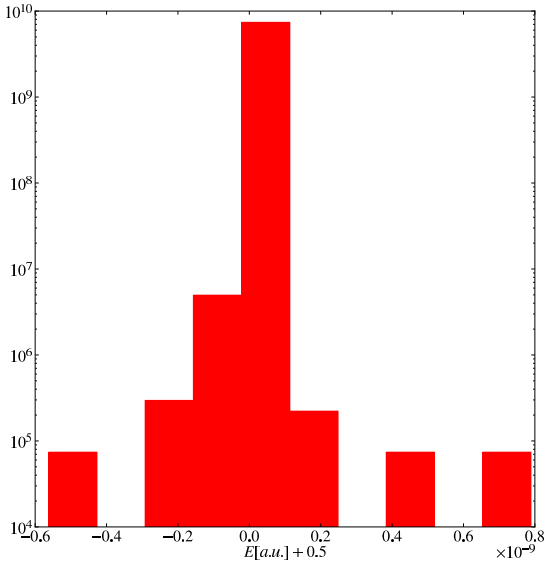

(a) Split Operator

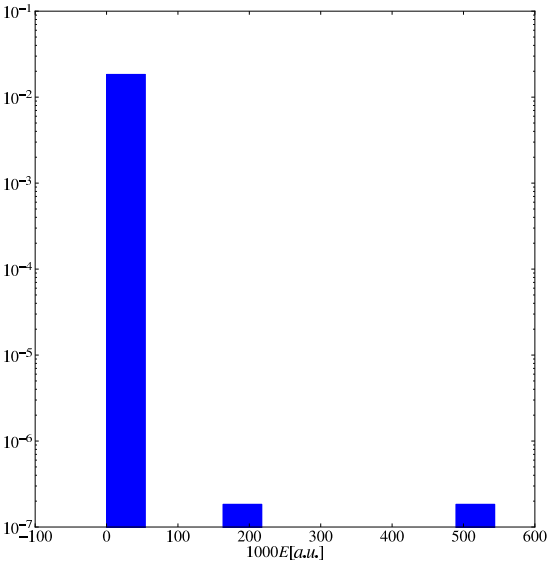

(b) Runge-Kutta, Implicit

Figure 3.3: Histogram of final energies for $E_{\max} = 0$ a.u. and step size $\Delta t = 0.000\,766\,99$ a.u., wave length of laser $\lambda = 3000$ a.u., Initial energy $E_0 = -0.5$ a.u., 100 000 samples, Simulation time $t_{\text{run}} = T_{\text{laser}}$, Comparison between the Strang-splitting Split-Operator scheme and the implicit and explicit 3rd oder Runge-Kutta methods on a hydrogen atom in a monochromatic laser field using dipole approximation; Note the different scales of each diagram, especially the Split-Operator figure 3.3a

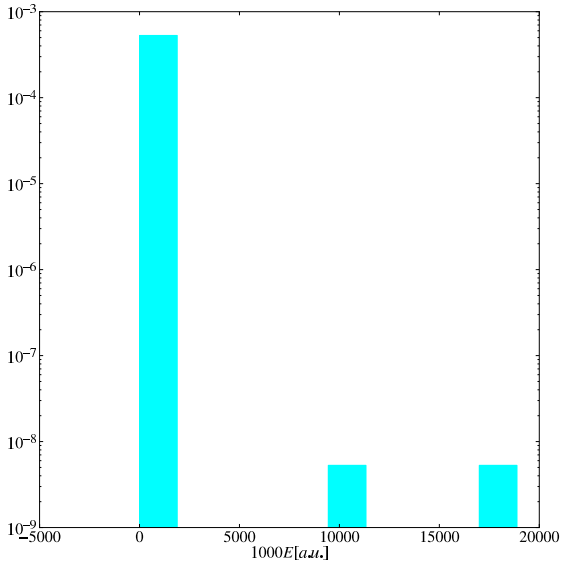

(c) Runge-Kutta, Explicit

Figure 3.3: Histogram of final energies for $E_{\max} = 0$ a.u. and step size $\Delta t = 0.000\,766\,99$ a.u., wave length of laser $\lambda = 3000$ a.u., Initial energy $E_0 = -0.5$ a.u., 100 000 samples, Simulation time $t_{\text{run}} = T_{\text{laser}}$, Comparison between the Strang-splitting Split-Operator scheme and the implicit and explicit 3rd oder Runge-Kutta methods on a hydrogen atom in a monochromatic laser field using dipole approximation; Note the different scales of each diagram, especially the Split-Operator figure 3.3a

Comparison of ionisation probability for different schemes and step sizes

The classical ionisation probability for the two Runge-Kutta and the Split-operator (Strang-splitting) schemes for an hydrogen atom in a laser field in dipole approximation is comparatively shown in 3.4.

Initially it can be said that the ionisation probability is increasing in a saturating curve to 1.0 for rising electrical field amplitude $E_{\max}$, which is to be expected. The saturation of the ionisation probability is reached at roughly $E_{\max} = 0.3$ for all numerical schemes with the exception of the Strang-splitting scheme's rate for the largest step size. The ionisation probability stays almost constant at roughly 0.8 and there is only a small rise to be see. The cause is that the step size is too large for the numerical approxiation performed to be valid hence this unphysical behaviour is displayed. Moreover one can see the sharper rise of the ionised amount begins at two times the barrier-suppression $E_{\max} = {}^{Z^2}/_{16}$ a.u. . All curves with the exception of the lowest step-size for the Split-operator curve for the largest step size are in agreement with the theoretical expectation that ionisation only starts for electric field strengths higher than the ionisaiton suppression barrier and saturates to 1.0 for high electric field strengths. However it is to be observed that the curvature is different for the three schemes and quantitative differences, especially in the regime lower than the ionisation supression barrier, are to be seen. The qualitative shapes of the graphs for reasonable step sizes are what is also to be seen in [5].

In figure 3.4a it is clearly observed that the Runge-Kutta integrators produce a higher amount of ionised particles than the Split operator scheme as displayed in figure 3.4b in the regime below two times the ionisation suppression barrier and to a smaller extend in the regime before saturation. The region below $E_{\max} = 0.1$ has a high amount of particles ionised that is not physically possible in the laser field considered. Additionally the ionisation probability shows a strong dependences on the step size for the numerical solution of the hydrogen atom in the monochromatic laser field in dipole approximation using the Runge-Kutta schemes. The step size still clearly has visible influences on the ionisation probability even at very tiny step sizes for the Runge-Kutta numerical schemes.

This is the result of the artificial ionisation caused by the low angular momenta problem the Runge-Kutta schemes suffer from. Artificial energy gain is induced by this phenomenon as discussed in more detail in the previous subsection. Hence the higher ionsation rate is a numerical artefact and implies a clear disadvantage of both Runge-Kutta schemes when solving the combined Kepler potential and laser field propagation. The unphysical gain of energy trajectories with low angular momentum artificially ionises particles. Moreover, the advantages of the symplectic implicit scheme over the non-symplectic explicit scheme are to be seen, as the explicit scheme suffers more from the numerical artefact of too high ionisation probabilitys. Much computational effort in the form of smaller step sizes needs to be made in order to achieve reliable results. Even for the smallest step size the Runge-Kutta schemes both still produce these numerical artefacts for $E_{\max}$ lower than two times the barrier-suppression field strength and to a lower extend before saturation

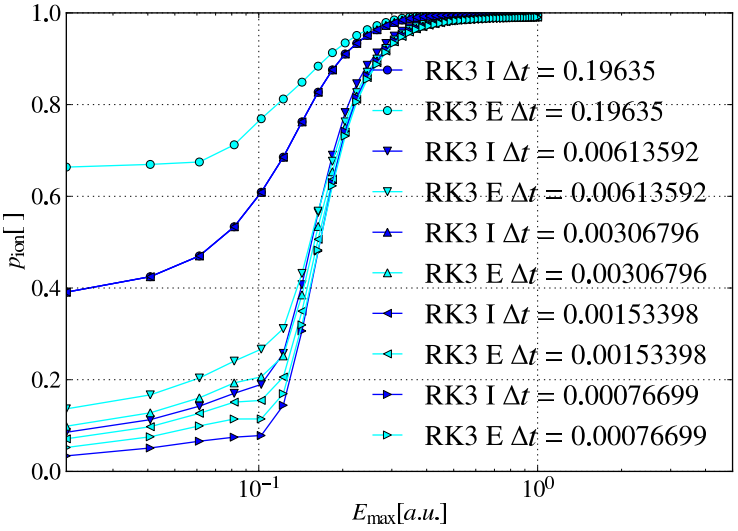

(a)

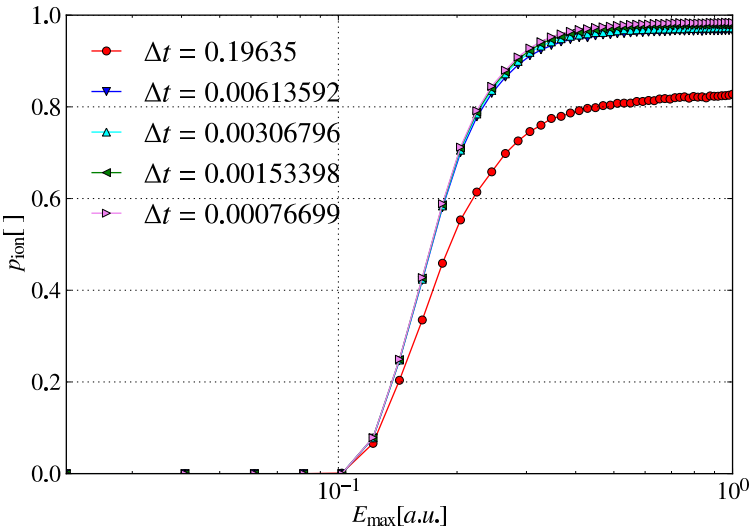

(b)

Figure 3.4: Ionisation probability p_{ion} over peak of electrical field strength E_{max}, wave length of laser $\lambda = 3000$ a.u., Initial energy $E_0 = -0.5$ a.u., 100 000 samples, Simulation time $t_{\text{run}} = T_{\text{laser}}$, all step sizes in atomic units, Comparison between the implicit and explicit 3rd oder Runge-Kutta method and Strang-splitting Split-Operator scheme on a hydrogen atom in a monochromatic laser field in dipole approximation; Note incomplete saturation for the largest step size for the Split-Operator scheme (step size too large) and the unphysically high ionisation probability for lower electrical field strength for the Runge-Kutta method; Also note the slightly different size of x-axis for both figures

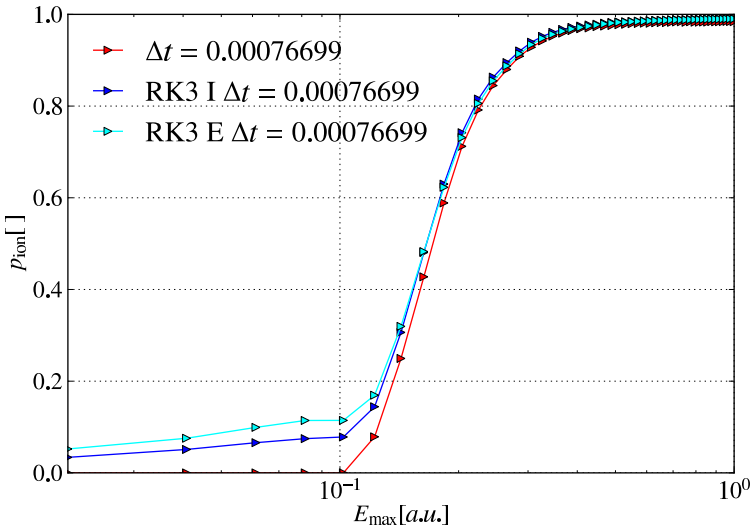

Figure 3.5: Ionisation probability p_{ion} over peak of electrical field strength E_{max}, wave length of laser $\lambda = 3000$ a.u., Initial energy $E_0 = -0.5$ a.u., 100 000 samples, Simulation time $t_{\text{run}} = T_{\text{laser}}$, all step sizes in atomic units, Comparison between the implicit and explicit 3rd oder Runge-Kutta method and Strang-splitting Split-Operator scheme all three using the smallest step size used on a hydrogen atom in a monochromatic laser field in dipole approximation

as displayed in figure 3.5. As the curve comes closer to saturation the agreement between the Runge-Kutta numerical classical ionisation probability and the Split-operator classical ionisaiton rate increases. Both schemes agree at least in the number of particles ionised. The agreement regime is to be found for $E_{\max} > 0.1$ a.u. for the tiniest step size used.

For the Split-Operator determined ionisaiton rate the picture is quite different as observed in figure 3.4b. The ionisation probability only begins rising after the passing of the two times ionisation barrier-suppression point. For the largest step size the saturation seems to tend to roughly 0.8 instead of the expected 1.0, indicating that the step size is just too large to properly render the numerical solution. The cause for this behaviour is that the expansion used to derive the Split-operator scheme that the time step is small is no longer valid for this step size. For all other chosen step sizes the expected saturation happens. Moreover there is very little change in the curve for smaller step sizes hence it can be deduced that a step- size of about 0.006 a.u. already gives reliable results. Hence the quality of the results using the Split-Operator method is better despite the fact that the order of magnitude of the numerical truncation error derived should be higher for the Split operator scheme. The two Runge-Kutta schemes have both an truncation error of $O(\Delta t^4)$ whereas the Split operator scheme (Strang-splitting) theoretically has an truncation error of $O(\Delta t^3)$. The low angular momentum problem and the fact that the Split operator method employed (Strang-splitting) is symplectic, preserves the symmetry, time-reversibility and the first order invariants of the system is the cause for this difference. Apart from the symplecticity of the implicit 3rd Runge-Kutta scheme employed here do not have these properties. The explicit Runge-Kutta scheme used even is not symplectic Hence these results support the conjecture that the Split-Operator integrator can achieve better results than a Runge-Kutta (explicit or implicit) integrator using the same step size. The main cause is that the numerical artefacts associated with low angular momenta not accounted for in the truncation error in the Runge-Kutta schemes.

In summary the Strang-splitting produces reasonable results for all step sizes but the largest, where the approximation used for the numerical integration is no longer valid. The Runge-Kutta schemes both always display too high ionisation probabilitys below the saturation regime of the ionsaiton rate which heavily depends on the step size. Quite tiny step sizes are needed to achieve results that are at least partially usable. That almost no ionisation occurs below two times the suppression-barrier is not rendered properly even for quite tiny step sizes for the numerically determined ionsation rates using the Runge-Kutta methods. Consequently the Strang-splitting numerical approach yields much more satisfactory results than the 3rd order explicit and implicit Runge-Kutta schemes of the ionsaiton rate for an hydrogen atom in a monochromatic laser field in dipole approximation.

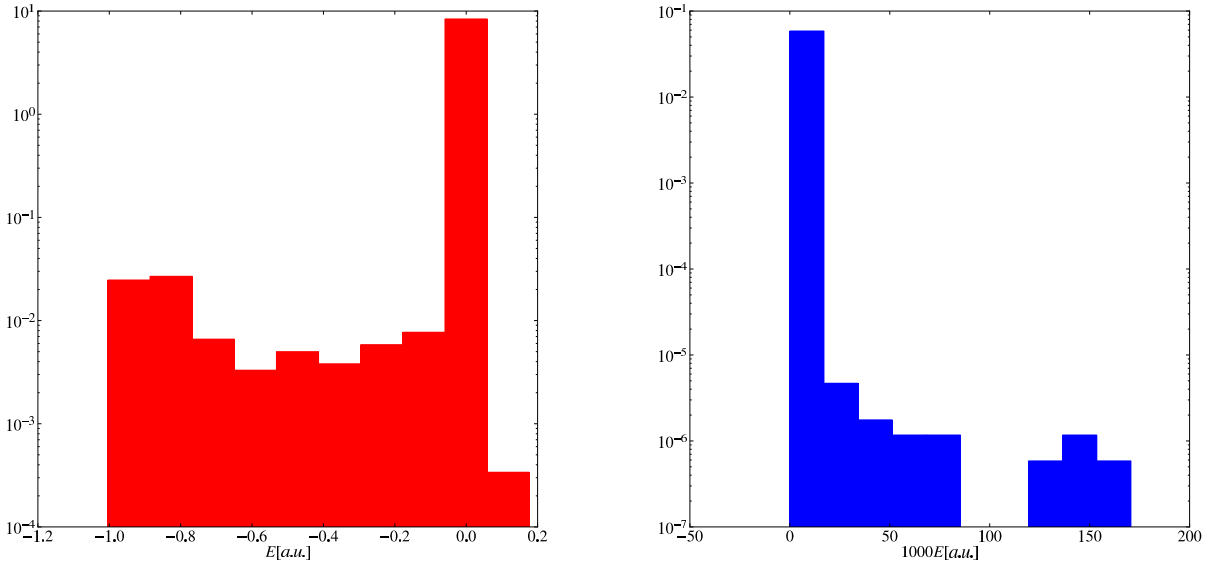

(a) Split Operator

(b) Runge-Kutta, Implicit

Figure 3.6: Histogram of final energies for $E_{\max} = 0$ a.u. and step size $\Delta t = 0.000\,766\,99$ a.u., wave length of laser $\lambda = 3000$ a.u., Initial energy $E_0 = -0.5$ a.u., 100 000 samples, Simulation time $t_{\text{run}} = T_{\text{laser}}$, Comparison between the implicit and explicit 3rd oder Runge-Kutta method and Strang-splitting Split-Operator scheme on a hydrogen atom in a monochromatic laser field in dipole approximation; Note the different scales of each diagram

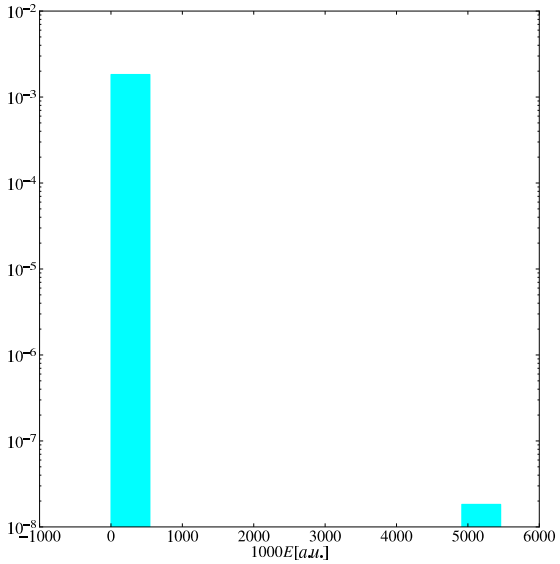

(c) Runge-Kutta, Explicit

Figure 3.6: Energy histograms for $E_0 = -0.5$ a.u., 100 000 samples, $\Delta t = 0.003\,067\,96$ a.u., $E_{\max} = 0.510\,204$ a.u.

Analysis of energy distributions for activated laser field

The histograms to be seen in figure 3.6 show the energy spreads for an amplitude roughly half of the chosen maximum of $E_{\max} = 1.0$ a.u. for the smallest step size used. In 3.6a it is to be seen that the Strang-splitting shows a spread of energies shifted to the right because of the laser field induced energy gain. Apparently some particles have gained some energy, however this is not dramatic. The particles ionised (i.e. with $E > 0$ a.u.) mostly reside in a regime of 0.0 a.u. $< E <$ 0.2 a.u. implying no physically impossible gain of energy. The microcanonical nature is, of course, not present as the laser field supplies additional energy to the system. Apart from some spread around the initial energy this histogram shows what is to be expected after the laser field with $E_{\max} = 0.5$ a.u. exposure on an ensemble of non-interacting particles in a keplerian potential. On the contrary the two Runge-Kutta schemes display a unphysical distribution of energies for an electric field amplitude of $E_{\max} = 0.5$ a.u. as to be investigated in 3.6b and3.6c. Almost no particles are still in the regime around the initial energy $E_0 = -0.5$ a.u. and most particles have a positive energy. The energy distribution calculated via the implicit 3rd order Runge-Kutta scheme to be investigated in 3.6b shows that some particles have gained an unphysical amount of energy. Nevertheless the amount of unphysical gain is not in an extremely high regime. The symplectic nature of the employed 3rd implicit Runge-Kutta scheme prevents a more serious unphysical augmentation

of energy. Oppositely the energy distribution determined by the explicit 3rd order Runge-Kutta scheme, presented in 3.6c, shows a tremendous increase in the energy of some particles compared to 3.6b. Moreover the number of particles with an unphysically high energy gain is larger than for the implicit scheme's energy distribution.

3.2.4 Performance tests on a local computer

The running times are the other issue which will be investigated. For that pupose the absolute running time was recorded on the local Computer supplied for this thesis by the MPIK. The Computer has an Intel©Core^{TM}i7 2600 (4x 3.5 GHz, HT^{TM}) and 16GB RAM. The reason why no more abstract research is made because the simple number of calls performed is not really something that can be compared between the two schemes as much different routines and algorithms are called and performed that vary in their execution time (e.g. fixed point iterations). Additionally measurement on the MPIK's cluster would have been difficult as the node(s) used always contain different processors and surrounding hardware. The results are comparable as the program's used have the same structure and were run on the same Computer which had no major other programs running. To achieve comparable results other programs were not run as much as possible. The parameters to test the running time were mostly set to those in the above simulations for a moderate step size. In 3.1 one can see that the explicit Runge-Kutta scheme has the shortest running time. This development is what one expects as the scheme has much less demanding computations than the other two. However one must think of the fact that the results it produces are very poor compared the the implicit scheme's and especially the Operator-Splitting scheme's results as shown in the analysis of the ionisation probability graphs for different step sizes. Even for much higher step sizes the explicit scheme shows problems especially for lower electric field amplitudes. The running time of the Split-Operator method has a running time roughly 38% higher than the explicit scheme. Nevertheless its results are much better than the explicit Runge-Kutta scheme's as seen in the analysis. As already mentioned the low electric field amplitude regime is rendered especially well. Moreover even the step size this test was run on is enough to achieve satisfactory results. The implicit scheme has an, comparably, immensely higher running time than the two other schemes. Its results are a bit better than the explicit scheme's, however the running time is much increasing quite profusely with a gain in precision not high enough. The problems in the lower electric field amplitude regime remain and smaller step sizes are not the remedy for it as the analysis shows.

In summary the Split-Operator scheme shows great advantages over the two standard Integrator schemes. The running time is a bit higher than the one of easy schemes, but on the contrary the results are much better. Even if the analytic solution of the Kepler problem is computationally demanding it is still much faster than symplectic schemes of the easiest kind and is able to produce much better results when employed in the Split-Operator technique. The Split-Operator scheme

Scheme	t_{program}
Split-Operator	56.6 s
RK3E	40.8 s
RK3I	169.8 s

Table 3.1: Runtime table $E_0 = -0.5$ a.u., 100 000 samples, $\Delta t = 0.006\,135\,92$ a.u., $E_{\max} = 0.5$ a.u.

is advantageous concerning both running time and satisfactory results implying a good performance of the scheme.

3.3 Simulations with Qprop

In order to be able to compare the results achieved with the classical schemes to a quantum mechanical approach, simulations with Qprop written by Dieter Bauer were performed. As it almost entirely matches what is wanted in order to carry out a simulation with parameters comparable to the classical results, the *hydrogen* example provided in Qprop was used in a modified version here. Main changes were:

- The pulse duration was chosen to one laser period T_{laser}
- The range of intensities was chosen exactly like in the classical experiments
- A term presumably describing the extension of the core as not needed for pure hydrogen
- The frequency of the laser was adjusted to a value corresponding to $\lambda = 3000$ a.u.

The rest of the parameters were left at the default values provided with the example. As described in 2.1 the projection onto the ground state that was initially calculated using imaginary time-propagation yielding p_{Ground} was conducted. Hence an upper bound for the ionisation probability can be found from the probability to find the electron in a state higher as the ground state given by $1 - p_{\text{Ground}}$.

3.3.1 Comparative experiment

The probability that the electron is not found in the ground state after propagation dependent on the amplitude of the electrical field determined in the Qrpop simulations are to be seen in 3.7. The general picture of a saturation curve is present in this figure as it was in the classical simulations. However the saturation regime is only reached at a peak electrical field strength $E_{\max}$ of about 3 a.u. . Furthermore the curve stays almost constant in the regime below $E_{\max} = 0.1$ a.u. . The absolute value in this regime is that high because even particles only excited to the first excited state of the hydrogen atom are not accounted for in the projection giving this quite high

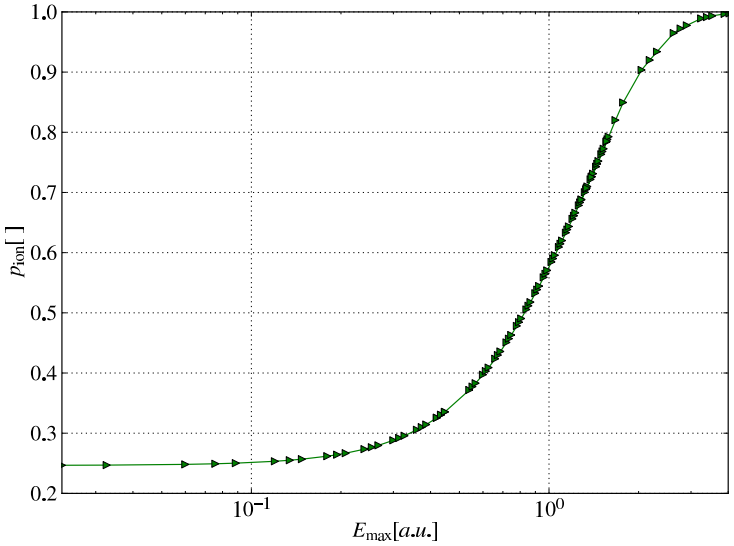

Figure 3.7: Probability $1 - p_{ground}$ not to find the electron in the ground state over peak of electrical field strength E_{max}, wave length of laser $\lambda = 3000$ a.u. Simulation time $t_{\text{run}} = T_{\text{laser}}$, $1s$ hydrogen ground state as determined by Qprop via imaginary time propagation as starting state, $t_{\text{run}} = T_{\text{laser}}$, Qprop simulation using the hydrogen example for a hydrogen atom in a monochromatic laser field in dipole approximation;

upper bound. To include more states one could determine wavefunctions of some lower excited state and subtract the projection of the final state onto them as well. As this would only opend a way to confirm wether the the quantum mechanical solution matches the classical Monte Carlo method in the region $E_{\max} < 0.1$ this was not done here.

In order to compare the obtained upper bound for the ionisation probability, as determined by the Qprop simulations, to the classical Monte Carlo simulations all curves were plotted into one diagram in figure 3.8. This is easily possible as curves depend on $E_{\max}$. This figure qualitatively shows that the upper bound is qualitatively matching the behaviour of an almost constant rate below $E_{\max} = 0.1$ a.u.. The non-constant behaviour of the ionisation probability approximated by a numerical integration using a 3rd order implicit Runge-Kutta scheme as well as an explicit Runge-Kutta scheme in this regime is caused by artificial ionisation processes induced by high velocities of core-close trajectories. This is a well known problem for the all Runge-Kutta methods and was proven to exist for the problem at hand discussed in more detail in the previous section. Yet another result of this problem is the higher ionisation probability of the Runge-Kutta integrators in that regime compared to the ionisation probability of almost zero for the numerical integration using a classical Split-operator technique known as Strang-splitting. Figure 3.8 implies a consistence between classical and quantum mechanical approach in the regime where $E_{\max} \leq 0.1$ a.u. as the lower bound for the ionisaton rate is not surpassed by the classical simulations. The Strang-splitting determined curve matches the qualitative behaviour of the upper bound more closely implying advantages of that scheme. In all schemes the curves display an qualitative increase from $E_{\max} = 0.1$ a.u. onwards. It becomes evident, however, that the Qprop-determined upper bound for the ionisation probability increases much more slowly than the classically Monte Carlo determined ionisation probability which shows a sharp increase starting at the electric field amplitude just discussed. This effect continues and the classical Monte Carlo ionisation probability surpasses the quantum mechanical upper bound at roughly $E_{\max} = 0.1$ a.u.. The classical ensemble determined ionisation rates than proceeds to saturate comparably quickly whereas the Qprop determined upper-bound for the ionisation probability saturates a lot slower and a lot later. This cannot be considered matching as the ionisation rate should not be higher than the upper-bound determined by Qprop if the Qprop simulation is considered to be correct. The lack of the inclusion of higher excited states in the projection cannot explain the quantitative disagreement as the inclusion of more excited states into the projection will only give a better upper bound for the ionisation probability that canot be larger than the ground stater determined one. The reason might be problems that are known to occur in the classical Monte Carlo method for certain wavelengths of the laser pulse that lead to a earlier saturation than the quantum mechanical solution yields. It is highly likely that this is indeed what is observed here as the qualitative shape of the upper-bound matches the Monte Carlo determined ionisation probability. The result of an analysis determining the probability the final wavefunction yields outside of some sphere around the nucleus would most probably yield sim-

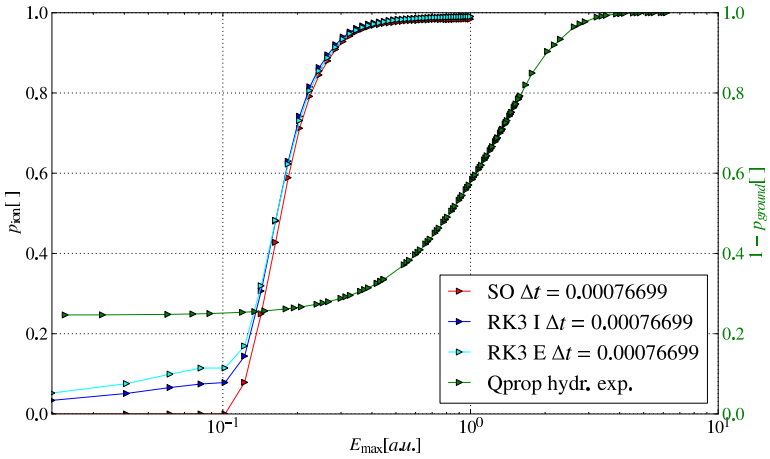

Figure 3.8: Ionisation probability p_{ion} over peak of electrical field strength E_{max}/Probability $1 - p_{ground}$ not to find the electron in the ground state over peak of electrical field strength E_{max}, wave length of laser $\lambda = 3000$ a.u. Simulation time $t_{\text{run}} = T_{\text{laser}}$, $1s$ hydrogen ground state as determined by Qprop via imaginary time propagation as starting state, $t_{\text{run}} = T_{\text{laser}}$, Qprop simulation using the hydrogen example for a hydrogen atom in a monochromatic laser field in dipole approximation; For the classical simulations: Initial energy $E_0 = -0.5$ a.u.and 100 000 samples, step size $\Delta t = 0.000\,766\,99$ a.u.

ilar results as the projection methods as the same wavefunction is used as a basis and excited states always have a bigger probability density in regions far away from the core than the ground state wavefunction yields resulting in similar results. Only tests with many wavelengths and parameters will be able to entirely enlighten this problem.

In summary the comparision to results obtained by pure quantum mechanics was regrettably not able to fully confirm the data obtained by the classical Monte Carlo simulation. For numeric integrations other than the splitting techniques the method employed using microcanonical ensembles of non-interacting particles is known to work. As the splitting technique is consistent with the Runge-Kutta integrations if a proper analysis of numerical artifacts is consistent the new splitting scheme can be considered a success.

4 Summary

The simplest variant of a symplectic classical operator-splitting technique, namely the Strang-splitting, was used to analyse the ionisation probability of a hydrogen atom in a laser field in dipole approximation using a classical Monte Carlo method simulating quantum mechanical behaviour. The points of comparison were a classical Monte Carlo simulation using an explicit and a symplectic implicit 3rd order Runge-Kutta scheme as an integrator as well as the quantum mechanical propagation of the groundstate of the hydrogen atom in a laser field using techniques implemented in the program qrop. As the considered regime is still in the non-relativistic range relativistic effects were thoroughly ignored. Furthermore all parameters chosen induce that the relativistic corrections would be that small that it is perfectly possible to neglect them.

Generally the Strang-splitting showed many advantages over the Runge-Kutta integration when solving the problem of an hydrogen atom in a monochromatic laser field in dipole approximation. The main advantage is the analytical solution of the Kepler problem as many standard integrators have difficulties. The main problem that appeared with the Runge-Kutta integration were problems concerning an artificial gain of energy not induced by physical effects, but by numerics resulting in ionised particles even without an activated laser field. This results might seem unexpected at first as the 3rd order explicit and implicit Runge-Kutta schemes have a smaller truncation error than the employed Strang-splitting revealing the fact that the truncation error is not the only error occurring in numerical integrations. The artificial energy gain is known to be caused by low angular momentum trajectories that involve high velocities at the part of the trajectory close to the core. Constant step-size Runge-Kutta schemes incorrectly render the velocity changes, resulting in a different trajectory corresponding to a higher total energy. Adaptive step size schemes are one remedy to these problems as the step size can be lowered, if the parameters are set right, whenever a high velocity region is entered. The performance of these schemes is, for example, researched in [11]. This analysis proved the adaptive schemes as quite advantageous. However research would be needed on how well these schemes deal with long term integration. A problem is that the symplectic properties of most implicit Runge-Kutta schemes are lost whenever non-constant step sizes are used (see e.g. [10]). This problem does not seem to be as severe as assumed (see again e.g. [11]) however the long term integration may hence turn out problematic as symplecticity is one of the major properties needed for stable long-term integration. A remedy to this issue is the development of symplectic numerical techniques that use adaptive time steps. One possibility is a rescaled time where the step size stays constant within the rescaled time, but not in real time.

An example that was tested in [11] is described in [16]. The scheme outlined there turned out to be most advantageous compared to all other unadaptive and adaptive Runge-Kutta schemes. Another advantage was that standard Runge-Kutta integrators could be used to numerically solve the transformed equations of motion resulting from the rescaled time. A comparison of these methods with the here employed splitting approach will be an interesting subject for investigation. As the splitting techniques have more advantageous properties for long term integration one would expect them to be superior in terms of precision and running time to the symplectic adaptive schemes if comparable truncation error schemes are used. However, solid proof for that is required to actually confirm this.

Symplectic integrators are suited to perform long-time integrations as they preserve the phase space volume (i.e. the total energy) when applied to systems described by Hamiltonian mechanics. Unphysical gain or losses in energy can hence be prevented to a certain degree because of the symplectic phase space volume conservation. This fact is advantageous for long term integration as gains or losses in energy caused by numerics tend to accumulate over time.

On the one hand it was found that the splitting techniques showed clear advantages over the Runge-Kutta schemes when determining the ionisation probability of a hydrogen atom in a monochromatic laser field described in dipole approximation. On the other hand it was not successfully possible to compare and match the quantum mechanical description to the classical description that uses a Monte Carlo method in order to imitate quantum mechanical behavior. One problem is that a deeper analysis of the quantum mechanical data obtained from Qprop is needed. More higher excited states should be included in the projections of the final wavefunction onto the bound states as here only the ground state was used. This would yield better information in the saturation regime, because if the electron is not in the ground state it is not necessarily ionised. Similarly a different analysis involving the probability to find the electron outside a sphere around the hydrogen nucleus as used in [5]. Another possibility is that the ionised parts of the wavefunction were not able to propagate away from the nucleus because the simulation was ended right after the laser pulse was over. However the upper bound for the ionisation probability obtained using Qprop shows a clear discrepancy in the regime above an amplitude of the electric field above $E_{\max} = 0.1$ where the lower bound is much lower than the Monte Carlo determined one. Additionally the saturation of the curve only occurs for much higher $E_{\max}$ as for the Monte Carlo data. The problem definitely is not the splitting technique used to solve the classical equations of motion as the Monte Carlo method employed here is known to work in most cases ever since Abrines and Percival suggested it in [4]. Nevertheless it is known that exactly the problem of later saturation and much higher electric fields needed for ionisation is known to occur for certain laser wavelengths combined with other parameters. It must be assumed that the choice of parameters must have induced this problem. To properly verify the correspondence many more experiments involving different wavelengths should be carried out in the future.

Despite the fact that a total verification of the approximate equivalence of quan-

tum mechanics and the Monte Carlo approach to determine ionisation rates was not possible the test of the splitting technique can be considered a success as the problems that occurred are known and the general use of the Monte Carlo method in that way is already proven. Especially the fact that the Runge-Kutta methods are known to properly render the system encourages that the splitting indeed works as it is clearly visible that the splitting technique's results match the Runge-Kutta determined ones. Differences in the low electric field amplitude could easily traced back to known issues of the Runge-Kutta schemes. The splitting method is able to numerically solve the problem in 3D without using things like a soft-core potential. One could also include the magnetic field into the splitting as the vector potential would only give additions to the Kick stage of the problem. An analytic solution of the Kick stage may become difficult then, however efficient numeric techniques or even a splitting into more parts could be employed.

4.1 Outlook

Apart from the task emerged after the data analysis to retest the equivalence to the quantum mechanical solutions the next step is to use higher order splitting methods than the Strang-splitting to obtain even more accurate results. Care should be taken that the higher order schemes also have the advantageous properties of the Strang-splitting (symplecticity symmetry-preserving, time-reversibility preservation and first order invariant preservation). Another interesting point of research is the inclusion of the magnetic field into the calculation to see how much more computational effort this costs. A boosting of the performance of the inclusion might be possible if splitting techniques involving more than one part are used. Again care should be taken to always chose schemes that have the ideal properties for long term integration. The inclusion of the magnetic field will widen the regions the splitting technique can be applied to as more parts of FIG. 1. of [9] become accessible.

To widen the accessible area in the diagram even further relativistic effects need to be taken into account. In order to achieve an analytical solution to the 3-dimensional relativistic Kepler problem needs to be found and implemented. The paper [17] is a starting point to develop such an algorithm. This would enable one to employ a proper relativistic treatment. A scheme like that would be very advantageous as numerical solutions obtained from the Dirac equation or the Klein-Gordon equation tend to be a lot more demanding considering computational resources than the numerical solutions of the Schrödinger equation. Moreover only the more demanding relativistic calculations need to be performed and not a combination of quantum mechanical calculations mixed with relativistic ones. The implementation and deeper analysis of a scheme like that would be very beneficial.

Bibliography

[1] Gerard A. Mourou, Toshiki Tajima, and Sergei V. Bulanov. Optics in the relativistic regime. *Rev. Mod. Phys.*, 78:309–371, Apr 2006.

[2] H. G. Hetzheim and C. H. Keitel. Ionization dynamics versus laser intensity in laser-driven multiply charged ions. *Phys. Rev. Lett.*, 102:083003, Feb 2009.

[3] R. Abrines and I. C. Percival. A generalized correspondence principle and proton-hydrogen collisions. *Proceedings of the Physical Society*, 88(4):873, 1966.

[4] R. Abrines and I. C. Percival. Classical theory of charge transfer and ionization of hydrogen atoms by protons. *Proceedings of the Physical Society*, 88(4):861, 1966.

[5] Heiko Bauke, Henrik G. Hetzheim, Guido R. Mocken, Matthias Ruf, and Christoph H. Keitel. Relativistic ionization characteristics of laser-driven hydrogenlike ions. *Phys. Rev. A*, 83:063414, Jun 2011.

[6] Donald H. Kobe. Gauge transformations and the electric dipole approximation. *American Journal of Physics*, 50(2):128–133, 1982.

[7] G.S. Balaraman and D. Vrinceanu. Numerical solution of modified-Kepler problem using a splitting method. *Physics Letters A*, 369(3):188 – 195, 2007.

[8] Dieter Bauer and Peter Koval. Qprop: A Schrödinger-solver for intense laser-atom interaction. *Computer Physics Communications*, 174(5):396–421, 2006.

[9] H. R. Reiss. Dipole-approximation magnetic fields in strong laser beams. *Phys. Rev. A*, 63:013409, Dec 2000.

[10] E. Hairer, C. Lubich, and G. Wanner. *Geometric numerical integration: structure-preserving algorithms for ordinary differential equations*. Springer series in computational mathematics. Springer, 2006.

[11] Fabian Klein. Anwendung von symplektischen Integratoren in klasssichen Monte Carlo Simulationen. Avaialble from the Theory section of the MPIK.

[12] Masuo Suzuki. Decomposition formulas of exponential operators and Lie exponentials with some applications to quantum mechanics and statistical physics. *Journal of Mathematical Physics*, 26(4):601–612, 1985.

[13] Daniel Condurache and Vladimir Martinui. A complete closed form vectorial solution to the Kepler problem. *Meccanica*, 42:465–476, 2007. 10.1007/s11012-007-9065-7.

[14] Harry Bateman. Haley's methods for solving equations. *The American Mathematical Monthly*, 45(1):pp. 11–17, 1938.

[15] William H. Press, Saul A. Teukolsky, William T. Vetterling, and Brian P. Flannery. *Numerical Recipes 3rd Edition: The Art of Scientific Computing*. Cambridge University Press, New York, NY, USA, 3 edition, 2007.

[16] Miguel Preto and Scott Tremaine. A class of symplectic integrators with adaptive time step for separable hamiltonian systems. *The Astronomical Journal*, 118(5):2532, 1999.

[17] T. H. Boyer. Unfamiliar trajectories for a relativistic particle in a Kepler or Coulomb potential. *American Journal of Physics*, 72:992–997, August 2004.

Erklärung

Ich versichere, dass ich diese Arbeit selbstständig verfasst und keine anderen als die angegebenen Quellen und Hilfsmittel benutzt habe.

Heidelberg, den …